

# Assessment of bauxite residue stabilized with lime and graphene oxide as a geomaterial for road applications

Ajay Jatoliya<sup>1</sup> , Subhojit Saha<sup>1</sup> , Bheem Pratap<sup>2</sup> , Somenath Mondal<sup>2</sup> ,  
Bendadi Hanumantha Rao<sup>1#</sup> 

Article

## Keywords

Tailings stabilization  
Bauxite residue  
Dual additives  
Strength  
Durability  
Road application

## Abstract

Negative traits of bauxite residue (*BR*) include low shear strength, inconsistent compaction characteristics and dispersion, render it unsuited geomaterial for engineering applications. The present study aims at stabilizing *BR* with the combination of lime (*L*) and graphene oxide (*GO*) in suitable proportions and investigating their impact on improvement in engineering properties (viz., density, unconfined compressive strength (*UCS*), dispersion, and durability). Lime of 2-10% and *GO* of 0.05-0.1% dosages (% weight of *BR*) are selected for experimentation purpose. Results demonstrate that *L* and *GO* together, not the individual additive, is effective to stabilize *BR*. A substantial improvement in *UCS* from 710 kPa of raw *BR* to 3890 kPa after treating with 10% *L* and 0.1% *GO* with 60 days curing period has been observed. 6% *L* and 0.05% *GO* for strength only in the short-term, and 10% *L* and 0.05% *GO* in durability aspect in the long-term are found as optimum dosages. Drastic decline in turbidity from 453 to 83 NTU establishes that *L* (6%) and *GO* (0.05%) addition completely alleviates dispersion behavior in *BR*. Though *GO* addition is trivial, its effect on strength and durability enhancement of *BR* is significant. Cementitious gel formations and bonding mechanism leading to particle aggregations are evidenced as the reason behind the improvement in strength and durability of *BR*. To verify the applicability of amended *BR*, the obtained findings are compared vis-à-vis with standards, which illustrated that the amended *BR* could be an excellent resource material in road construction, especially in base or sub-base courses.

## 1. Introduction

Primary problems in the use of bauxite residue (*BR*) as a construction material are lower shear strength, collapse potential, and dispersion (Mishra et al., 2020b). Past research has established that the strength of *BR* is very low owing to the presence of an excessive quantity of monovalent sodium ( $\text{Na}^+$ ) ions, which hinder particle flocculation (Reddy et al., 2021a, b; Reddy & Rao, 2018; Zhang & Tao, 2008). The dispersion behavior of *BR* makes it vulnerable to severe erosion (Reddy et al., 2016a, 2018, 2021b; Singh et al., 2020). Thus, addressing the strength and dispersion becomes key problems when *BR* is to be considered as a construction material. Alongside, *pH* above 10 and the possible leaching of toxic elements under severe alkaline circumstances are a few more deterrents for the low volume usage of *BR* (Singh et al., 2020; Zhang et al., 2018, 2020a).

On the other hand, road construction requires a substantial quantity of resource materials, which are acquired from naturally available resources. In view of the excessive exploitation of nature and natural resources, the conversion of waste materials into usable geomaterials by appropriately stabilizing them with additives seems promising. *BR* is one of the potential materials that could be devised as an alternative to naturally depleting materials. Dual problems of low strength and dispersion of *BR* can be alleviated by amending with suitable additive(s) such that the modified residue meets the requirement when it is to be employed for constructing embankments, rural roads, making of bricks and paving blocks, and developing *BR* based geopolymer products (Reddy et al., 2016b; Zhang et al., 2020b; Zhao et al., 2019, 2020). Zhang et al. (2016) have developed a composite material using *BR* and slag with improved strength characteristics. Jha et al. (2020) have investigated the possibility of using *BR* to stabilize expansive soils to be used in clay lining system. Kumar & Kumar (2013) have conducted research

<sup>#</sup>Corresponding author. E-mail address: bhrao@iitbbs.ac.in

<sup>1</sup>Indian Institute of Technology Bhubaneswar, School of Infrastructure, Bhubaneswar, Odisha, India.

<sup>2</sup>National Institute of Technology Jamshedpur, Department of Civil Engineering, Jharkhand, India.

Submitted on April 15, 2022; Final Acceptance on November 4, 2022; Discussion open until May 31, 2023.

<https://doi.org/10.28927/SR.2023.003722>



This is an Open Access article distributed under the terms of the Creative Commons Attribution License, which permits unrestricted use, distribution, and reproduction in any medium, provided the original work is properly cited.

on the utilization of *BR* in conjunction with other industrial by-products such as fly ash to produce paving blocks. On a pilot project scale, Kehagia (2008) has used *BR* for the development of a soil subgrade and road embankment.

Lime is documented as a highly effective additive for treating a range of geomaterials in the field of soil stabilization (Mishra et al., 2020a). Its treatment impacts consistency, compaction, strength, swelling, and dispersion characteristics of various types of problematic soils such as black cotton soil and organic soil (Ajayi, 2012). This can be linked to the versatility and heterogeneity as well as the variety of mineralogical properties of lime (Farhan et al., 2020). A typical comparison of the effect of lime with cement indicates that the improvement of shear strength in lime stabilized soil lasts for more than two years, whereas the latter additive effect continued only for six months (Al-Rawas et al., 2005). In this context, lime could be a potential additive to stabilize the *BR*. Based on the systematic review of literature, another important knowledge gap that the authors identified is poor understanding of the effect of curing time on lime stabilization. In the knowledge of authors, there are a few literatures available that discusses the influence of lime on *BR*. Table 1 elucidates the studies as regards to treatment of *BR* with calcium rich waste materials or lime.

Nano-sized elements, such as graphene oxide, have recently become popular as cementitious composites to improve the mechanical properties of soils. The use of graphene oxide (*GO*) in civil engineering applications has recently seen a significant upsurge in light of its merit as an additive to cementitious material. The review of literature reveals that majority of *GO* applications are remain confined to cement and concrete, either to improve strength (Gong et al., 2015; Liu et al., 2019), freeze-thaw resistance (Mohammed et al., 2016); porosity (Mohammed et al., 2015); workability (Indukuri et al., 2020) or durability (Priya et al., 2021). *GO* has also successfully been introduced as part of a hybrid additive to improve the performance of construction materials (Gao et al., 2019; Pateriya et al., 2021). Liu et al. (2018) used *GO* in hot mix asphalt binder for three types of warm mix additives and reported an increase in viscosity, deformation resistance, and elasticity at high temperatures

in the *GO*-modified mixes. A greater degree of interfacial adhesion between *GO* and cement mix might explain the significant strength increment of the resultant mix.

It appears from the literature that a few efforts are devoted to explore the usability of *GO* in soil and waste material stabilization. Zhu et al. (2010) have noticed that liquid limit, plastic limit, and plasticity index of the cement-treated soil samples declines as *GO* concentration increases. The addition of *GO* to cement-treated soil resulting in an increment of unconfined compressive strength and shear strength has been reported by Naseri et al. (2016). Strength improvement, reduced compressibility and hydraulic conductivity are all factors in the development of the treated soil (Kai et al., 2019; Pateriya et al., 2019; Zhu et al., 2010).

The review of literature pertinent to *BR* suggests that it can be stabilized using lime, cement, and other pozzolanic additives with variable success rates. The majority of studies emphasize that it is necessary to stabilize the *BR* with more than one type of additive, bearing in mind multiple problems as aforementioned. There are no studies to the knowledge of authors that employ lime and graphene oxide, in tandem, to improve the geotechnical properties of *BR*. The present research focuses on evaluating the performance of *L* and *GO* in different proportions together to stabilize the *BR*. The efficacy is assessed in terms of compaction parameters and strength. In addition to the mechanical studies, durability properties of stabilized *BR* are evaluated. The results outlined in the paper have practical implications in terms of encouraging the use of *BR* in road construction as a base/subbase material, backfill material in geotechnical structures, and geomaterial in construction sector.

## 2. Materials and testing methodology

Bauxite Residue used in the present study was collected from the waste disposal pond of Vedanta Aluminium Limited, located at Lanjigarh in Kalahandi, Odisha, India. The samples collected were in wet and disturbed state and were collected from 1 m depth at the pond to ensure homogeneous sample collection. Soon after the collection, the wet samples were oven dried and pulverized with wooden mallet to prepared

**Table 1.** Description and contribution of studies pertinent to treatment of *BR* with calcium rich waste materials.

| Reference                | Brief description of study  | Major contributions/observations  |
|--------------------------|---|---|
| Anastasiou et al. (2014) | Mechanical strength of bricks made from calcareous fly ash and red mud mix.   | Increment in percentage of fly ash led to increment in mechanical strength of brick block in 28 days.                                   |
| Kumar & Prasad (2019)    | Effect of water content, ratio of water to lime, dry density and ratio of porosity to lime on the <i>UCS</i> of lime stabilized <i>BR</i>                         | Increment in <i>UCS</i> with an increase in lime content.   |
| Aswathy et al. (2019)    | Compaction behaviour, <i>UCS</i> , <i>CBR</i> value of soil stabilized with red mud and lime  | Introduction of lime to <i>BR</i> stabilized clay soil improved <i>CBR</i> , <i>MDD</i> , and <i>UCS</i> values.                        |
| Mishra et al. (2019)     | Comparison between the effect of lime only treatment and lime with organic acids treatment on compaction characteristics, <i>UCS</i> and <i>pH</i> of <i>BR</i> . | Characteristics of treated <i>BR</i> improved when the treatment was performed with both lime alone and lime and organic acid together. |

the samples for subsequent laboratory testing programmes. Laboratory tests for establishing geotechnical properties including, specific gravity (*G*), gradational characteristics, consistency limits, compaction characteristics, alkalinity (*pH*), and classification were performed following ASTM codes. Table 2 presents the results of the aforementioned tests on *BR* samples.

To examine the effect of lime (*L*) and graphene oxide (*GO*) treatment on the strength parameters of the *BR*, commercial-grade *L* and *GO* were purchased from the Golchha enterprises, Jamshedpur. The dosage selected for lime were 0, 2, 4, 6, 8, and 10% and that of *GO* is 0, 0.05, and 0.1% (by basis of % dry weight of *BR*). The choice of dosage of lime is based on study by Satyanarayana et al. (2012), who have showed a steady increment in *UCS* up to 10% of lime dosage. Similarly, the above dosage of *GO* is decided such that the resultant produce is cost effective. Table 3 shows sample combinations along with designations for which laboratory experiments were performed.

Initially, standard Proctor compaction tests were performed for the aforementioned combinations as per ASTM (2007d) standard. Unconfined compressive strength (*UCS*) tests were carried out on stabilized samples as per the ASTM (2007a). A series of samples for the combinations shown in Table 2 were prepared by compacting to maximum dry unit weight ( $\gamma_{dmax}$ ) at optimum moisture content ( $w_{opt}$ ). The prepared samples were placed in the polybags to prevent moisture loss and cured for 7, 21, 45, and 60 days. Another identical set of samples was prepared for durability testing purposes. Each stabilized sample for durability test was initially cured for 7 days at an ambient condition and thereafter, it was immersed in water for 4 hours. After continuous 4 hours of immersion in water, *UCS* of the sample was measured. As there are no specified guidelines available to determine the durability of stabilized waste materials, values specified in the IRC: SP 89 (IRC, 2018) were referred to.

**Table 2.** Physical properties of bauxite residue used for the study.

| Sl. No. | Property                             | Value |
|---------|--------------------------------------|-------|
| 1.      | <i>G</i>                             | 3.09  |
| 2.      | Atterberg's limit (%)                |       |
|         | Liquid limit ( $w_L$ )               | 40    |
|         | Plastic limit ( $w_p$ )              | 29    |
|         | Plasticity index ( <i>PI</i> )       | 11    |
| 3.      | % Fraction                           |       |
|         | Sand                                 | 18    |
|         | Silt                                 | 56    |
|         | Clay                                 | 26    |
| 4.      | Compaction characteristics           |       |
|         | $\gamma_{dmax}$ (kN/m <sup>3</sup> ) | 16.6  |
|         | $w_{opt}$ (%)                        | 28    |
| 5.      | <i>pH</i>                            | 12.5  |
| 6.      | USCS classification                  | ML*   |

\*Inorganic silts of slight plasticity.

Additionally, dispersion tests (crumb tests) on the stabilized samples were conducted, as per ASTM (2019). For testing purposes, cylindrical samples were prepared with a length-to-diameter ratio of two, similar to that needed for *UCS* test according to ASTM (2007c). The samples were visually observed and photographed for any disintegration effect. The disintegrated particles from the sample affect the turbidity of the water. Hence, the turbidity of the water was measured using a Hach 2100N turbidity meter. Finally, *pH* of all the stabilized samples was measured according to ASTM (2007b).

To verify the inter-particle bonding and cementation effects of stabilized *BR* with *L* and *GO*, Scanning Electron Microscope (*SEM*) analysis was performed. It is to be noted that the *SEM* analysis was conducted on those stabilized samples, which were already subjected to *UCS*. Thus, curing periods remain common across samples used for *SEM* and *UCS*. A small portion of the stabilized soil was separated from the middle of soil core and was coated with a thin layer of gold for two minutes using Hitachi E-1010 Ion Sputter at a vacuum of 6 Pa before the analysis. The gold coating facilities to reveal the best morphological characteristic of the sample, simultaneously avoiding charging problems during testing.

To establish mineralogical compositions of the stabilized samples, X-Ray Diffraction (*XRD*) analysis was performed. For this purpose, sample grabbed from the stabilized soil core that was already subjected to *UCS* test was used. It was then oven dried at 105 °C for 24 hours, ground to powder form and sieved through 75 µm sieve. 4 g of this powder sample was scanned for 2θ ranging from 5 ° to 70 ° (Bragg angle) with a step increment of 0.01 ° and a time of 0.5 s/step size using a copper X-ray tube (Cu-Kα) at current and voltage of 30 mA and 40 kV.

**Table 3.** Mix proportions with designation of *BR* samples adopted in the study.

| Sl. No. | Mix proportion                         | Mix designation |
|---------|--|-----------------|
| 1.      | Raw <i>BR</i> +0% Lime+ 0% <i>GO</i>   | RBR             |
| 2.      | <i>BR</i> + 2% Lime + 0% <i>GO</i>     | R1              |
| 3.      | <i>BR</i> + 4% Lime + 0% <i>GO</i>     | R2              |
| 4.      | <i>BR</i> + 6% Lime + 0% <i>GO</i>     | R3              |
| 5.      | <i>BR</i> + 8% Lime + 0% <i>GO</i>     | R4              |
| 6.      | <i>BR</i> + 10% Lime + 0% <i>GO</i>    | R5              |
| 7.      | <i>BR</i> + 2% Lime + 0.05% <i>GO</i>  | R6              |
| 8.      | <i>BR</i> + 4% Lime + 0.05% <i>GO</i>  | R7              |
| 9.      | <i>BR</i> + 6% Lime + 0.05% <i>GO</i>  | R8              |
| 10.     | <i>BR</i> + 8% Lime + 0.05% <i>GO</i>  | R9              |
| 11.     | <i>BR</i> + 10% Lime + 0.05% <i>GO</i> | R10             |
| 12.     | <i>BR</i> + 2% Lime + 0.1% <i>GO</i>   | R11             |
| 13.     | <i>BR</i> + 4% Lime + 0.1% <i>GO</i>   | R12             |
| 14.     | <i>BR</i> + 6% Lime + 0.1% <i>GO</i>   | R13             |
| 15.     | <i>BR</i> + 8% Lime + 0.1% <i>GO</i>   | R14             |
| 16.     | <i>BR</i> + 10% Lime + 0.1% <i>GO</i>  | R15             |

### 3. Results and discussion

#### 3.1 Effect of $L$ and $GO$ on compaction properties

Dry unit weight ( $\gamma_d$ ) versus moisture content ( $w$  %) relationships are developed for raw  $BR$  as well as  $BR$  treated with varying proportions of  $L$  is shown in Figure 1. It is seen from the figure that  $\gamma_{dmax}$  decreased and  $w_{opt}$  increased with an increase in lime content, except corresponding to 2%. Generally, lime imbibes water for hydration. As the lime content increases, water requirement for its hydration increases. It is however can be noted that the reaction of lime with water is exothermic in nature. As a result, some part of water generally gets evaporated during the reaction process. These statements can be linked to an increase in  $w_{opt}$  with an increase in lime content.

Figure 2 represents the variation of  $\gamma_{dmax}$  and  $w_{opt}$  with a change in dosage of lime. It is evident from Figure 2 that there is a continuous decrease in  $\gamma_{dmax}$  and an increase in  $w_{opt}$  with increment of lime dosage. The maximum and minimum values of  $\gamma_{dmax}$  and  $w_{opt}$  are measured as 16.9 and 15.1 kN/m<sup>3</sup> at 26.1 and 32.2% respectively. When lime content is increased from 2 to 10%,  $\gamma_{dmax}$  decreased from 16.9 to 15.1 kN/m<sup>3</sup> whereas  $w_{opt}$  increased from 26.1 to 32.2%. Though lime content of 2% has yielded the highest values of  $\gamma_{dmax}$  and  $w_{opt}$ , trend lines of these parameters merged at a lime dosage of 6%. Thus, 6% of lime dosage is used for experimentation to understand the effect of  $L$  and  $GO$  hybrid additive in  $BR$ . It is also obvious that  $\gamma_{dmax}$  value of 16.3 kN/m<sup>3</sup> meets the density requirement as prescribed by IRC 89 (IRC, 2010) for various civil engineering applications. The results in Figure 2 corroborate well with earlier studies by Mishra et al. (2019) and Ajayi (2012), who have stabilized the bauxite residue and soil using lime and noticed a decline in  $\gamma_{dmax}$  with simultaneous increase in  $w_{opt}$ .

Similarly, Figure 3 depicts compaction curves established on  $BR$  for  $GO$  content of 0, 0.05, and 0.1% against a fixed  $L$  dosage of 6%. It is seen that  $\gamma_{dmax}$  increased and  $w_{opt}$  decreased with an increase in  $GO$  content. The reason behind the increment of density and decrement of moisture content can be explained by Lambs' theory. According to which, at low water content, attractive forces between the particles are stronger than repulsive forces. Hence, soils compacted at moisture content less than optimum moisture content have a flocculated structure (Zhu et al., 2010).

An increment of moisture content increases the repulsive forces. The soil compacted at moisture content more than  $w_{opt}$  usually has a dispersed structure. It can be observed an improved compaction characteristic of  $BR$  samples when different percentages of  $GO$  (0, 0.05, and 0.1%) are incorporated but by keeping constant amount of lime (6%). The  $\gamma_{dmax}$  value increased from 16.3 to 17.5 kN/m<sup>3</sup> and  $w_{opt}$  decreased from 30 to 27%. These observations excellently confirm the study by Naseri et al. (2016), who

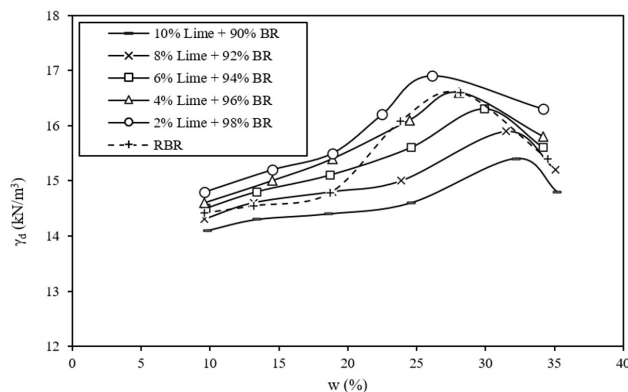


**Figure 1.** Relationship between dry unit weight and moisture content of untreated and lime treated bauxite residue samples.

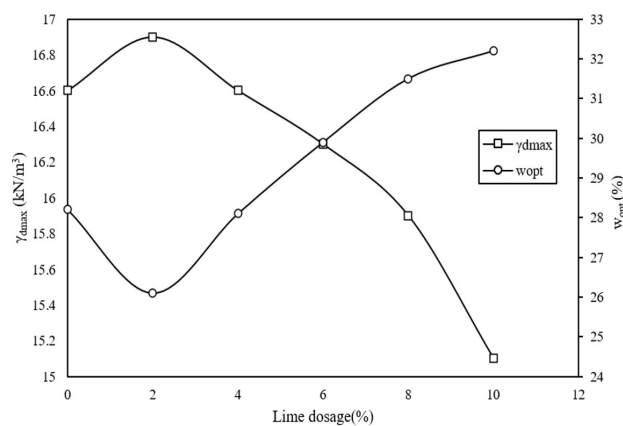


**Figure 2.** Variation of  $\gamma_{dmax}$  and  $w_{opt}$  with lime dosage.

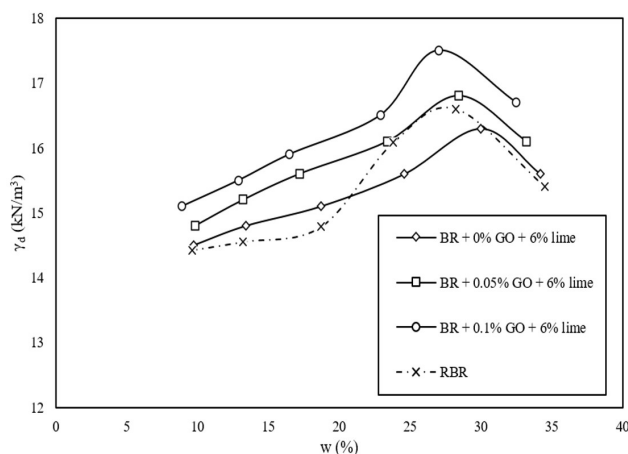


**Figure 3.** Compaction curves for  $BR$  amended with graphene oxide at lime dosage of 6%.

have illustrated an increase in  $GO$  quantity in the soil sample increases  $\gamma_{dmax}$ , while lowering  $w_{opt}$ . The increment of  $\gamma_{dmax}$  is not only consistent but also meets IRC SP: 20-2002 (IRC, 2002) recommendations for road construction applications, as it prescribes a minimum value of 16.19 kN/m<sup>3</sup>.

The increase in dry unit weight can be attributed to interaction between *GO* and cementitious compounds formed by the reaction of lime with *BR*. As *GO* acts as nuclei sites for hydration products, its presence plays an important role in the formation of thicker crystals with denser growth, which have a capability to intertwine *BR* particles (Zhu et al., 2010). The decrement in  $w_{opt}$  can be attributed to interface bonding between *GO* and cementitious products, as well as decrement of pores in samples. Corroborating the same, Naseri et al. (2016) have reported similar results of increment in  $\gamma_{dmax}$  and decrement in  $w_{opt}$  when *GO* sheets are added to soil/cement matrix. Confirming the above delineations, Lima et al (2017) have demonstrated a similarity in the hydration reaction occurring due to the admix of *BR* to calcium hydroxide to that of reaction between cement and water. On similar lines, Gordon et al. (1996) have highlighted the possible production of cementitious compounds including C-S-H gels when lime is added to *BR*. However, the quantity may comparatively low as reactive silica content in *BR* is relatively low and strength improvement of the matrix may also be due to formation of calcium aluminates (CA, possibly  $C_5A_3$ ) as well through the leftover alumina in *BR*. Mishra et al. (2019) have performed the *XRD* analysis on lime treated *BR* and illustrated the generation of cementitious compounds in presence of water. The results of *XRD* analysis performed in the present study, which will be discussed in the later section, also confirm the generation of various cementitious materials when lime and *GO* are added to *BR*.

It is a proven fact that *BR* contains high alkaline content and predominance of iron oxide, which is unusually greater than in normal soils. Thus, the impact of these variables on compaction parameters must be thoroughly understood, as there are no earlier studies that focused on such impacts

of these variables on compaction properties. In the present study, compaction curves, as presented in Figure 1, clearly show that treated *BR* is sensitive to the moisture content. This implies that *BR* requires more compaction energy to achieve desirable outcomes.

Validation of the compaction characteristics in Figures 1 and 3 with the literature shows that these trends are quite similar to other wastes (Reddy & Rao, 2018), except for non-ferrous slags, which exhibits extremely high  $\gamma_{dmax}$  at little  $w_{opt}$ . The findings in Figures 1 and 3 suggest that admix of *L* and *GO* together apparently overwhelms the extreme alkalinity and high iron content effects. It is also evident from the curves that the effect of *GO* is more vivid than *L* as regards to compaction properties of *BR*.

Understandably, the effect of *GO* on compaction characteristics of *BR* is quite opposite to that treatment with lime only. When used latter additive alone there is a continual decrement of density and increment of moisture content, which will not fetch any advantage. The *GO* content in the present study is limited to 0.1% bearing in mind the cost of this material. Demonstrably, the compaction results when compared vis-à-vis with different code recommendations portray that the combination of *L* and *GO* is doable to stabilize the highly alkaline bauxite residue.

### 3.2 Dispersion behavior

The performance of the *L* and *GO* combination on dispersion, is checked by crumb tests that are carried out on samples prepared by varying *GO* dosages (0, 0.05, and 0.1%) and lime of 0-10%. Corresponding to 0% *L* plus *GO*, the sample is considered a control test. Images of *BR* samples immersed in water after treating with *L* and *GO* are presented in Figure 4.

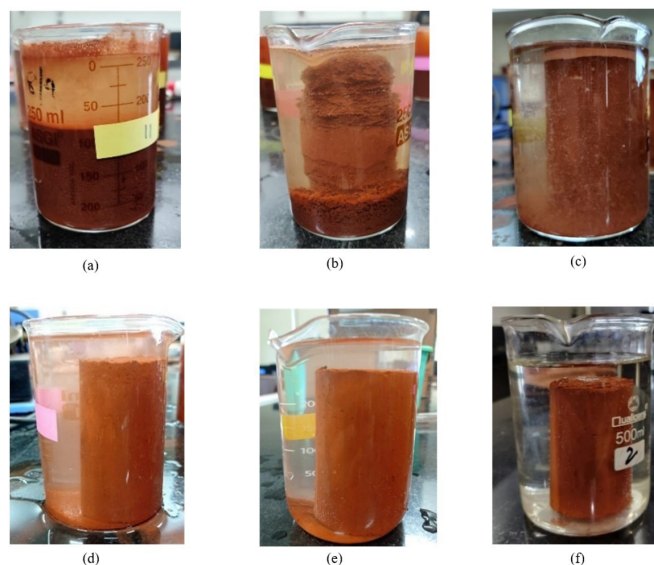


**Figure 4.** Pictures of *L* and *GO* amended *BR* samples after subjected to crumb tests: (a) raw *BR*, (b) *L*=2% and *GO*=0.05%, (c) *L*=4% and *GO*=0.05%, (d) *L*=6% and *GO*=0.05%, (e) *L*=8% and *GO*=0.05%, and (f) *L*=10% and *GO*=0.05%.

As is evident from the results illustrated in Figure 4, the untreated sample (Figure 4a) is heavily dispersed, resulting in dark and cloudy water inside the beaker. Whereas samples treated with increasing dosage of  $L$  and  $GO$  showed recession in dispersion behavior (Figure 4b and Figure 4f). The density of suspended particles decreased in which samples treated with  $L$  and  $GO$  are immersed, as the solution in these beakers became clearer. Stable samples with less disintegration of particles can also be seen with an increase in dosage of  $L$  and  $GO$ . Further to ascertain the dispersion behavior, change in turbidity of the solution is measured, as shown in Figure 5.

The turbidity value of untreated  $BR$  is measured as high as 453 NTU (Nephelometric turbidity unit). A continual decrement in turbidity for higher dosage of  $L$  and  $GO$  indicates the ability of these additives in mitigating the dispersion behavior of  $BR$  samples. However, there are no specific guidelines in the literature that link turbidity to dispersion activity. Therefore, no proposition is made about the optimum dosage of  $L$  and  $GO$  combination. Incidentally,  $L$  of 6% and  $GO$  of 0.05%, and  $L$  of 10% and  $GO$  of 0.1% have yielded significantly lower values of turbidity of 88 and 14 NTU.

Dispersion is a phenomenon that occurs in soil when it has a sizeable amount of exchangeable sodium ions (Li et al., 2021; Mishra et al., 2020a). Dispersion behavior in the  $BR$  appears to be exacerbated by the deficiency of clay particles and the existence of substantial sodium ions concentration. Compared to the presence of monovalent excess  $Na^+$  ions in the  $BR$ , concentrations of these divalent cations are exceedingly limited, resulting in the dispersive character (Reddy et al., 2019). As evident from Figure 4, dispersion activity in  $BR$  is decreased. This may be linked to the predominance of  $Ca^{2+}$  ions with the addition of lime. Divalent cations ( $Ca^{2+}$  and  $Mg^{2+}$ ) might have mitigated the dispersion by lowering the flocculation state. As the dosage of  $GO$  is increased, as it includes many hydroxyl groups that are formed by hydrogen bonding between the network of hydrogels and free water, there is a decrement in turbidity value.  $GO$  can also form a cross-linkage with calcium. The vast network of hydrogels, hydrogen bonding, and gel formed by cross-linking of  $GO$  with calcium all work together to improve particle binding and thereby, decline dispersion behavior in  $BR$  (Kai et al., 2019).

### 3.3 Effect of $L$ and $GO$ on UCS

$UCS$  measured on  $BR$  samples stabilized with varying proportions of  $L$  and  $GO$  (refer to Table 2 for designation of mixes) for short (7 & 21 days) and long-term (45 & 60 days) curing periods are presented in Figure 6 in the form of bar chart.

A remarkable improvement in  $UCS$  of treated samples can be noticed, highlighting the performance as well as the effectiveness of  $L$  and  $GO$  together for stabilizing highly alkaline wastes like  $BR$ . The variation of  $UCS$  is also fairly distinct between  $L$  and  $GO$ . It can be seen that as curing period increases so does  $UCS$  value. It is observed that the

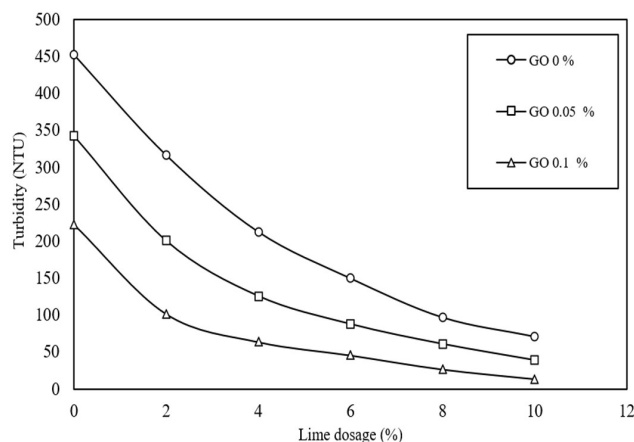


**Figure 5.** Turbidity test results of  $BR$  after treating with varying percentages of  $L$  and  $GO$ .

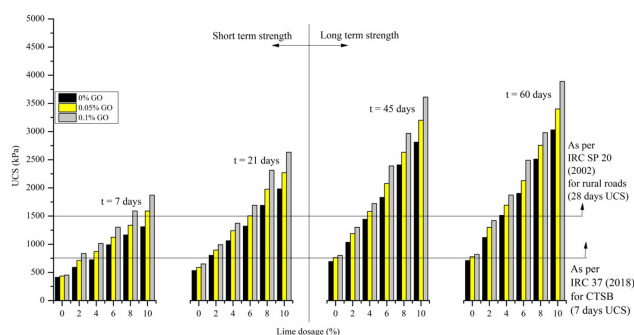


**Figure 6.** Measured compressive strength of  $BR$  samples amended with varying percentages of  $L$  and  $GO$  at different curing periods.

strength attained by untreated  $BR$  on 7<sup>th</sup>, 21<sup>st</sup>, 45<sup>th</sup>, and 60<sup>th</sup> day of curing is 412, 532, 692, and 710 kPa. Where as, those  $BR$  samples treated with 10%  $L$  and 0.1%  $GO$  attained a maximum strength of 1871, 2635, 3612, and 3890 kPa on the 7<sup>th</sup>, 21<sup>st</sup>, 45<sup>th</sup>, and 60<sup>th</sup> day of curing. The improvement in  $UCS$  is 4.54, 4.95, 5.22, and 5.47 times the strength of untreated  $BR$  sample. The considerable increment in strength is a strong indication that the amended  $BR$  complies with the code provisions for a specific engineering application. Bearing this in mind, an attempt is made to find out the field applications of stabilized  $BR$  in various civil engineering applications, as discussed herein.

As such, Indian Road Congress (IRC) SP:20 (2002) recommends a minimum  $UCS$  value of 1500 kPa of the chemically stabilized waste after 28 days of curing to be used in sub-base or base course of rural roads. Similarly, the required minimum  $UCS$  value according to IS-37 (2018) at 7 days for cement-treated sub-base (CTSB) is 750 kPa. Evidently, many combinations of mixes meet the above requirement of minimum  $UCS$  as per the IRC codes. Incidentally, the strength attained in the long-term default conforms to or even exceeds the strength requirement of sub-base and base

course of rural roads and chemically treated sub-base course for pavements. However, the base course of flexible pavement requires to have a minimum of 4500 kPa of UCS value in 7 days. *L* of 10% and *GO* of 0.1% have produced UCS of 3890 kPa after 60 days, which is nearer to the required value of 4500 kPa, though it is unable to accomplish the desired strength. Higher dosage of *L* and *GO* might enhance the strength beyond 4500 kPa. However, such combination might increase the overall cost of the construction. Thus, in terms of cost economics, it is prudent to choose the lower percentage of *L* and *GO* combination. Understandably, combinations of *L* of 6% and *GO* of 0.05% in the short-term (UCS value of 1504 kPa after 21 days) and *L* of 4% and *GO* of 0.05% (UCS value after 60 days is 1581 kPa) in the long-term produced a minimum strength of 1500 kPa, which renders suitability of the samples as resource materials for sub-base and base course of rural roads.

### 3.4 Durability properties

The durability test is conducted to identify the stability of the material under diverse environmental conditions. Figure 7 presents the durability test results for different mix combinations. It is observed that mixed proportions of R1, R2, and R3 have either collapsed or are unable to retain their shape in water. Hence, UCS tests are not conducted on these samples. Samples treated with 8 and 10% *L* maintain their shape and size and produced adequate results after 4 hours of immersion.

From Table 4 and Figure 7, it is evident that samples R4 to R10 displayed a significant decrease in strength, as is true that the ratio of UCS of immersed samples to non-immersed samples is calculated as < 80%. As per IRC: SP:

89 Part-1 (2010), if the strength ratio is < 80% such samples are unfit to be recommended for road construction purposes. It can be witnessed that mixes from R10 to R15 exhibited the strength that is greater than 80% of the strength of samples that are not plunged in water. Such combinations satisfy the a fore mentioned criteria and thus, they may be considered as regards to the durability. Further from the durability viewpoint, it can be stated that *L* of 10% and *GO* of 0.05% can be considered optimum dosage, as it fulfills the minimum strength requirement.

Figures 6 and 7 establish that when only the lime content and combination of *L* and *GO* in *BR* is increased, UCS improvement is striking. Clearly, the increase in mechanical strength is obvious before and after dipping in water, where the before state indicates strength in the short-term and the after state indicates durability in the long-term. As the silica content

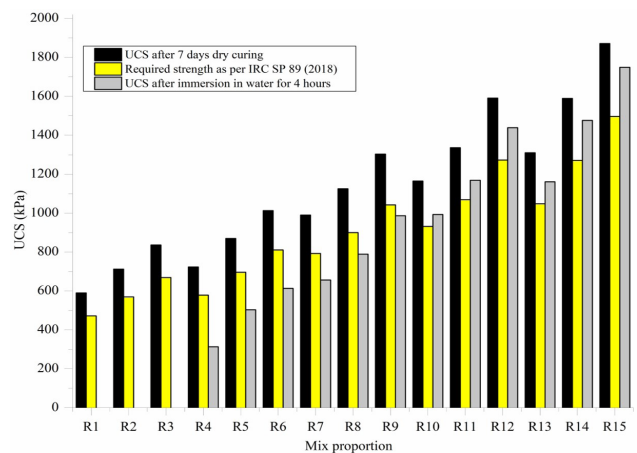


Figure 7. Comparison of UCS measured before and after immersion of treated BR samples in water.

Table 4. The value of UCS measured from mechanical and durability tests.

| Mix proportion | UCS (kPa) at 7 days without immersion in water | UCS (kPa) after 7 days of curing followed by immersion in water for 4 hours | Immersed UCS as a percentage of UCS without immersion (%) |
|----------------|--|---|---|
| R1             | 590  | Failed  | -   |
| R2             | 712  | Failed  | -   |
| R3             | 836  | Failed  | -   |
| R4             | 723  | 313   | 43.29   |
| R5             | 870  | 503   | 57.82   |
| R6             | 1013   | 613   | 60.51   |
| R7             | 990  | 656   | 66.26   |
| R8             | 1125   | 789   | 70.13   |
| R9             | 1303   | 987   | 75.75   |
| R10            | 1165   | 993   | 85.24   |
| R11            | 1336   | 1169  | 87.50   |
| R12            | 1591   | 1439  | 90.45   |
| R13            | 1310   | 1161  | 88.63   |
| R14            | 1589   | 1476  | 92.89   |
| R15            | 1871   | 1749  | 93.48   |

in BR is reportedly low, amount of generated cementitious products can understandably low when admixed lime alone. Hence, the increment in *UCS* is also lower when only *L* is added to *BR*, as evident from Figure 6. Results from study by Satayanarayana et al. (2012) shows a steady increase in *UCS* of lime treated *BR* and it postulates that this increase is due to the interaction between silica and alumina of *BR* and lime mix. Intriguingly, the introduction of *GO* to the matrix seemingly generated additional strength in the treated *BR* samples. At this juncture, the addition of *GO* together with *L* largely might have aided to attain higher strength of the desired level, as can be witnessed that strength of *L + GO* combination samples are pointedly higher vis-à-vis with those samples treated only with *L*. Generation of cementitious products due to reaction of *L* and *BR* (Gordon et al., 1996) and subsequent reaction of the cementitious and hydration products with *GO* is postulated to be contributing to the higher strength of the *BR* modified with the combination of *L* and *GO*. It is even interesting to note that a very modest addition of *GO* has greatly contributed to strength and durability enhancement, as is true from Figures 6 and 7.

### 3.5 *pH* of lime and graphene oxide stabilized *BR* samples

Table 5 shows the value of *pH* measured on *BR* samples stabilized with *GO* and *L* at various combinations and curing periods. The *pH* of raw *BR* is measured as 12.5. A glance at the results illustrates that the addition of *L* and *GO* has led to only a trivial reduction in *pH* of treated samples (the lowest observed *pH* is 11.8) against 12.5 of *RBR*, even after curing period of 60 days. A minute change in *pH* emphasizes that there are no obvious impacts, in terms of environmental, on the stabilized *BR*.

**Table 5.** The value of *pH* measured of amended *BR* samples at different curing periods.

| Mix designation | <i>pH</i> after different curing periods |        |         |         |         |
|-----------------|--|--------|---------|---------|---------|
|                 | 0 day                                    | 7 days | 21 days | 45 days | 60 days |
| RBR             | 12.5                                     | 12.45  | 12.3    | 12.4    | 12.4    |
| R1              | 12.43                                    | 12.40  | 12.34   | 12.30   | 12.25   |
| R2              | 12.38                                    | 12.35  | 12.20   | 12.22   | 12.18   |
| R3              | 12.30                                    | 12.24  | 12.18   | 12.12   | 12.08   |
| R4              | 12.26                                    | 12.16  | 12.10   | 12.01   | 11.90   |
| R5              | 12.25                                    | 12.10  | 12.02   | 12.00   | 11.88   |
| R6              | 12.5                                     | 12.40  | 12.33   | 12.22   | 12.16   |
| R7              | 12.45                                    | 12.39  | 12.20   | 12.18   | 12.11   |
| R8              | 12.36                                    | 12.28  | 12.11   | 12.02   | 11.92   |
| R9              | 12.30                                    | 12.22  | 12.16   | 12.13   | 12.00   |
| R10             | 12.25                                    | 12.04  | 12.12   | 11.96   | 11.88   |
| R11             | 12.47                                    | 12.32  | 12.23   | 12.05   | 11.91   |
| R12             | 12.39                                    | 12.30  | 12.22   | 12.18   | 12.01   |
| R13             | 12.30                                    | 12.12  | 12.05   | 11.90   | 11.88   |
| R14             | 12.25                                    | 12.11  | 12.01   | 11.94   | 11.85   |
| R15             | 12.20                                    | 12.01  | 11.90   | 11.85   | 11.80   |

The primary reason for the small change in *pH* can be linked to the fact that both *L* and *RBR* have *pH* values in the same range which is nearly 12-12.5. Hence, the addition of lime does not affect the *pH* of treated samples. The quantity of *GO* available in treated samples is also minimal. This may be a reason why there is an insignificant change in the *pH* of treated samples.

### 3.6 Mineralogical and morphological analysis

An attempt further is made to understand and confirm the improvement in strength, durability, and dispersion by confirming the mineralogical compositions of *BR* treated with *L* alone and that with *L* and *GO* by *XRD* analysis. Mix designated as R3 (*BR + 6% L*) and R8 (*BR + 6% L + 0.05% GO*) are considered for the analysis, as these are found to be the optimum dosage from the perspective of strength, compaction and dispersion. Figure 8 shows the X-Ray diffractogram patterns after identifying the dominant minerals and cementitious compounds.

Major mineralogical compositions identified in *BR* are Hematite (ICSD #01-089-8103), Boehmite (ICSD #01-083-2384), Sodalite (ICSD #01-089-9099), Calcite (ICSD #01-072-1652), Cancrinite (ICSD #01-089-8047) (Mishra et al., 2019, Castaldi et al., 2008). Incidentally, all these mineral compositions are identified in R3 and R8 samples. Additionally, cementitious and hydration products namely, Portlandite (ICSD #00-044-1481), Calcium silicate hydroxide hydrate (*CSHH*) (ICSD #00-026-0307), Di-calcium silicate (*C<sub>2</sub>S*) (ICSD #00-031-0302), Tricalcium aluminate (ICSD #00-038-1429), and calcium aluminate silicate hydrate (*CASH*) (ICSD #01-085-1567) are also found. Apart from these, a peak belonging to iron aluminate silicate (ICSD #01-082-1546) is also identified in both the samples. Presence of these cementitious and hydration products well affirm the increment in *UCS* of lime and *BR* mix at 7 and 28 days (Figure 6) besides the chemical reaction between calcium present in the lime and silica present in the *BR* (Kai et al., 2019). These inferences further prove the hypothesis that the mixture of *BR* and calcium hydroxide is similar to that of reaction between cement and water (Lima et al., 2017; Satayanarayana et al., 2012). However, a marginal difference in peaks is seen between R3 and R8 demonstrating that mineralogical compositions of both the matrix are nearly same. Although intensity of di-calcium silicate is visibly higher in case of R8, which reinforces the idea that due to addition of *GO* to the matrix, it helps in accumulation of cementitious and hydration products as the nanomaterial additive acts as nuclei for the cementitious products.

As per the Kai et al. (2019), the mechanism behind strength improvement when *GO* along with cement is admixed to unstabilized material, is a reaction of calcium silicate hydrate (*C-S-H*) and  $\text{Ca(OH)}_2$  which are products formed after the hydration of cement, with carboxylic acid groups on *GO* particles. It is stated that the contact produces

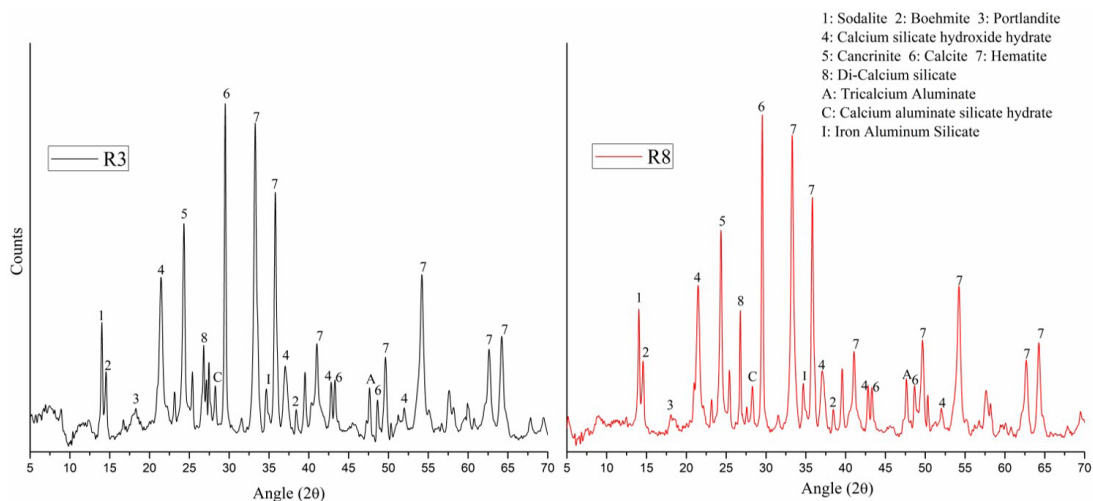


**Figure 8.** X-ray diffractogram patterns of *BR* samples stabilized with *L* alone (R3) and *L* + *GO* (R8).

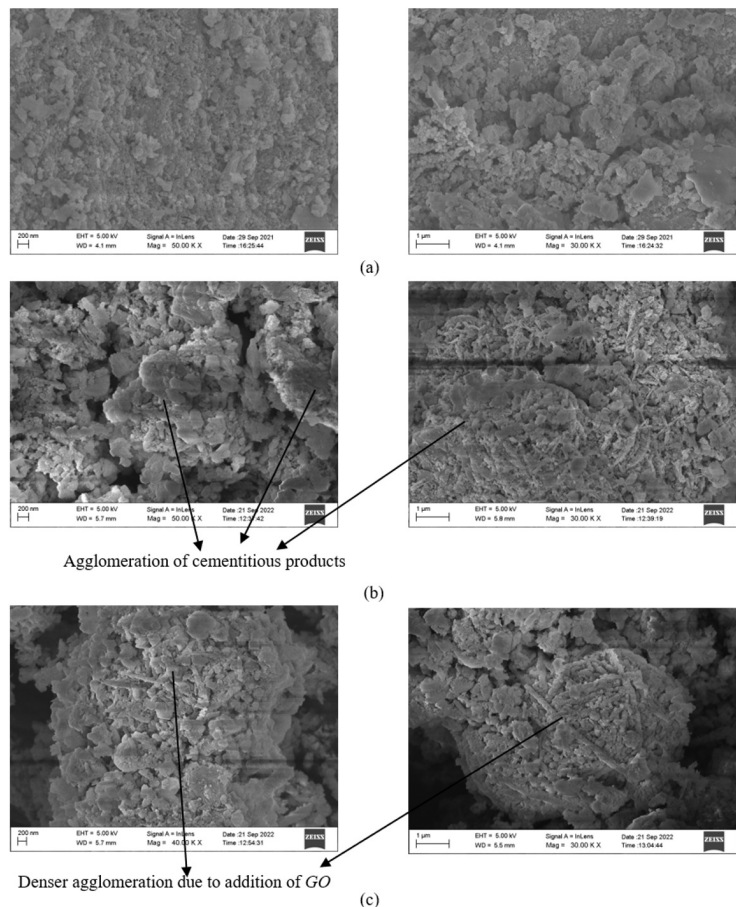
a strong covalent connection at *GO*-composite interface, which improves load-transfer efficiency from the cement matrix to the *GO* and consequently improves the composite's mechanical characteristics. Whereas in the study by Wan & Zhang (2020), it is elaborated that the chemical reaction occurs at the interface between *GO* and cementitious gels leads to an increase in Young's modulus as well as concentration of gel formations under alkaline environment. Contrary to C-S-H as reported by Kai et al. (2019), *CSSH* and *CASH* are found in the *L* and *GO* treated samples in the present study (Figure 8). Thus, it can be inferred that the reaction of *CSSH*, *CASH* along with  $\text{Ca}(\text{OH})_2$  with carboxylic acid groups on *GO* might be occurring in the *L* and *GO* treated samples. Further, the study by Pateriya et al. (2019) demonstrates that *GO* is a nanomaterial additive and it plays an important role in filling the pores within the matrix by providing nucleation sites. The prevalence of strong covalent bonding, increased Young's modulus and the activity of pore filling might have led to imparting additional strength to the matrix through creation of dense compact structure and further improvement in the durability properties, as reported in Figures 6 and 7.

Addition of *L* and *GO* also introduces refinement in morphology of treated *BR* samples. For this purpose, morphological features of treated *BR* samples have been established by *SEM* analysis. Figure 9 depicts *SEM* images captured on *RBR* and that amended with *L* of 6% only and *L* of 6% with *GO* of 0.05%. These mix proportions are chosen based on the conclusions derived from the foregoing results and discussion. Visual observations reveal a higher degree of particle agglomerations of *L* stabilized *BR* (Figure 9b) as compared with *RBR* (Figure 9a). Generation of *CSSH* and other cementitious products in the treated *BR* microstructure can be postulated as the reason for agglomerations in the matrix when lime is added to *BR*. Generally, the generated crystals are clustered to create bundles that result in pore filling and crystal overlapping. Since the *BR* and *L* promote

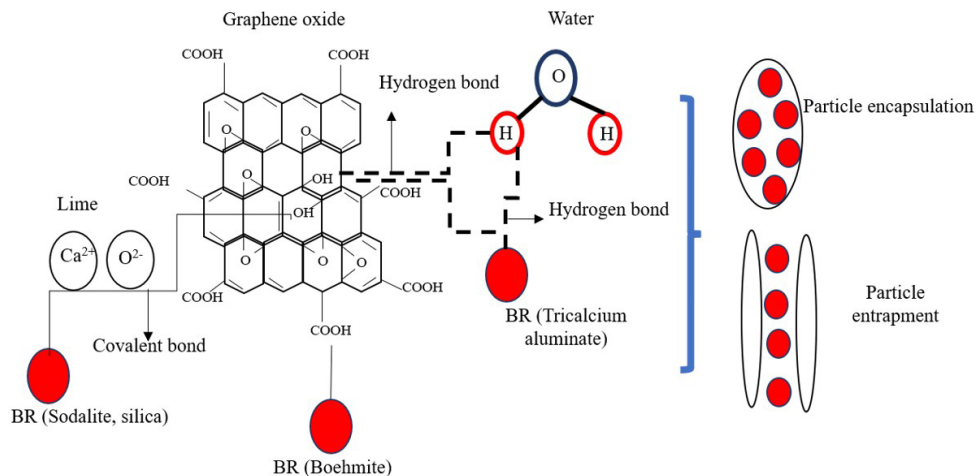
the pozzolanic reaction, the mineral structure of *L* stabilized *BR* has changed to the agglomerated columnar mixture, as is evident from Figure 9b. These phenomena well justify the improvement in strength in the short-term period (Figure 6) and durability in the long-term (Figure 7) simultaneously descending dispersion behavior (Figure 5).

Figure 9c shows the densified aggregation of cementitious products after adding *GO* to the mixture and they adhere each other tightly. When *GO* is introduced in the matrix, it fills the pores and acts as a nuclei to the cementitious products, resulting the mixture continue to develop, gradually becoming thicker and form the circular shape, and eventually agglomerate to cover the pores (Kai et al., 2019). They may also cross-link with calcium present in lime, allowing the substance to convert into the gel. The combination of the vast network of cementitious products such as Portlandite, Tricalcium aluminate, Dicalcium silicate, Calcium aluminum silicate hydrate, and Calcium silicate hydroxide hydrate along with *GO* resulted in an improvement in particle binding, bonding and aggregation. These processes well rationalize the strength and durability improvement in the long-term period (Figures 6 and 7).

Bonding of the particles can exist in several ways in the resultant matrix of *L* and *GO* stabilized *BR*. To delineate the same, a conceptual schematic has been drawn, as shown in Figure 10. Boehmite [ $\text{AlO}(\text{OH})$ ] can replace the carbon in the  $\text{COOH}$  group to form bonding between *BR* particles and *GO*. Hydrogen bonds can develop through hydroxyl ions in water with *GO* sheets, as is shown in Figure 10. These hydrogen bonds can also exist through the bonding of *GO* and water present in tricalcium aluminate ( $3\text{CaO}\cdot\text{Al}_2\text{O}_3\cdot 6\text{H}_2\text{O}$ ) (refer to Figure 8) generated due to the reaction between *BR* and lime in presence of water. Generally, water decomposes into hydroxyl ions ( $\text{OH}^-$ ) and hydrogen ions ( $\text{H}^+$ ) when a mixture of water, *BR*, *L*, and *GO* is admixed, by virtue of their chemical nature. The decomposed hydroxyl ions from



**Figure 9.** Morphological changes captured by SEM of *L* and *GO* amended bauxite residue samples, (a) raw *BR*, (b) *BR* treated with 6% *L*, and (c) *BR* treated with 6% *L* and 0.05% *GO*.



**Figure 10.** Conceptual diagram showing *BR*, *GO*, and *L* interaction.

water as well as from broken edges of *GO* sheets can combine with calcium oxide to generate Portlandite  $[Ca(OH)_2]$  (refer to Figure 8). This leads to a constant generation of  $OH^-$  in the matrix. Further sodalite  $(3Na_2O \cdot 3Al_2O_3 \cdot 6SiO_2 \cdot Na_2SO_4)$  in *BR*

will continue to react with  $Ca(OH)_2$  to create *CSHH* in the presence of opulent hydroxides. Aluminum oxide and free sodium ions present in the *BR* can also react with hydroxyl ions to produce aluminum hydroxide  $[Al(OH)_3]$  and sodium

hydroxide (NaOH). These compounds encapsulate the *BR* particles within the gel substance or entrap the particles by adherence. Figure 10 illustrates the encapsulation and entrapment mechanism of *BR* particles and the consequent aggregation process, as visualized from SEM images depicted Figure 9. Such consequences excellently corroborate the strength and durability increment with the addition of *L* and *GO* together, as reported in Figures 6 and 7, and mitigation of dispersion as illustrated in Figure 5.

## 4. Conclusions

This study presents a novel viewpoint on the effective amendment of the extremely alkaline *BR* and demonstrates that the lime and graphene oxide combination are necessary and could be considered as potential stabilizer combination. The various results show that lime and *GO* can significantly improve the strength and durability characteristics concurrently declining the dispersion behavior of bauxite residue. It is important to note that though the addition of *GO* is trivial, it yet contributed for successful conversion of *BR* into usable geomaterial. The study finds that 6% *L* + 0.05% *GO* in strength, compaction and dispersion perspective and 10% *L* + 0.05% *GO* in durability perspective are found as optimum dosages. The strength attainment of 3031 kPa with 10% *L* alone and 1500 kPa with 6% *L* + 0.05% *GO* surpass the acceptability criteria of IRC SP: 20-2002 and IRC 37:2018, indicating that the stabilized *BR* could be a rich resource material for constructing base and sub-base layers of rural roads and subbase of flexible pavements. The crumb test results reveal that the addition of small amount of *L* and *GO* greatly helped in stability i.e. retention of shape and prevention of collapse or dispersion, of *BR* samples. The morphological analysis visibly displayed encapsulation and entrapment of particles by gel structures and inter-particle binding and bonding in the treated *BR* samples. Overall, the study complements the utilization of bauxite residue as a road construction material. Nevertheless, the strength properties of bauxite residue with amendments under extreme climatic conditions (such as drought and freeze-thaw) including leaching characteristics are also worth exploring in the future studies.

## Declaration of interest

The authors have no conflicts of interest to declare. All co-authors have observed and affirmed the contents of the paper and there is no financial interest to report.

## Authors' contributions

Ajay Jatoliya: conceptualization, investigation, methodology, data curation. Subhojit Saha: conceptualization, investigation, data curation, formal analysis, validation, writing – original draft. Bheem Pratap: data curation, formal

analysis, validation, writing – original draft. Somenath Mondal: conceptualization, supervision, writing – review & editing. Bendadi Hanumantha Rao: conceptualization, supervision, writing – review & editing.

## Data availability

The datasets generated analyzed in the course of the current study are available from the corresponding author upon request.

## List of symbols

|                 |                                    |
|-----------------|------------------------------------|
| <i>BR</i>       | Bauxite residue                    |
| <i>CASH</i>     | Calcium Aluminate Silicate Hydrate |
| <i>CSHH</i>     | Calcium Silicate Hydroxide Hydrate |
| <i>G</i>        | Specific Gravity                   |
| <i>GO</i>       | Graphene Oxide                     |
| <i>L</i>        | Lime                               |
| <i>NTU</i>      | Nephelometric turbidity unit       |
| <i>pH</i>       | Potential of Hydrogen              |
| <i>PI</i>       | Plasticity index                   |
| <i>UCS</i>      | Unconfined compressive strength    |
| $w_L$           | Liquid limit                       |
| $w_{opt}$       | Optimum moisture content           |
| $w_p$           | Plastic limit                      |
| <i>XRD</i>      | X-ray Diffraction                  |
| $\gamma_{dmax}$ | Maximum dry density                |
| <i>ML</i>       | low plasticity silt                |

## References

- Ajayi, E.S. (2012). Effect of lime variation on the moisture content and dry density of lateritic soil in Ilorin, Nigeria. *International Journal of Forest, Soil and Erosion*, 2(4), 159-162.
- Al-Rawas, A. A., Hago, A. W., & Al-Sarmi, H. (2005). Effect of lime, cement and Sarooj (artificial pozzolan) on the swelling potential of an expansive soil from Oman. *Building and Environment*, 40(5), 681-687.
- Anastasiou, E.K., Papayianni, I., Konopissi, S., & Papachristoforou, M. (2014). Fly ash-red mud mixtures for masonry block production. In *1<sup>st</sup> Concrete Innovation Conference*, Oslo, Norway.
- ASTM D1633. (2007a). *Standard test methods for compressive strength of molded soil-cement cylinders* (pp. 1-15). ASTM International, West Conshohocken, PA.
- ASTM D4972. (2007b). *Standard test methods for pH of soils*. In ASTM International (Ed.), *Annual Book of ASTM Standards* (Vol. 1, No. 10, pp. 10-12). ASTM International, West Conshohocken, PA.
- ASTM D2166-87. (2007c). *Standard test method for unconfined compressive strength of cohesive soil*. ASTM International, West Conshohocken, PA.

- ASTM D698-07. (2007d). *Standard test methods for laboratory compaction characteristics of soil using standard effort*. ASTM International, West Conshohocken, PA.
- ASTM D6572-13e2. (2019). *Standard test methods for determination of dispersion characteristics of clayey soils by the crumb test*. ASTM International, West Conshohocken, PA.
- Aswathy, M., Salini, U., & Gayathri, V. G. (2019). Utility of lime and red mud in clay soil stabilization. In V. Stalin & M. Muttharam (Eds.), *Geotechnical characterisation and geoenvironmental engineering* (pp. 19-26). Cham: Springer.
- Castaldi, P., Silveti, M., Santona, L., Enzo, S., & Melis, P. (2008). XRD, FTIR, and thermal analysis of bauxite ore-processing waste (red mud) exchanged with heavy metals. *Clays and Clay Minerals*, 56(4), 461-469.
- Farhan, K.Z., Johari, M.A.M., & Demirboğa, R. (2020). Assessment of important parameters involved in the synthesis of geopolymer composites: a review. *Construction & Building Materials*, 264, 120276.
- Gao, Y., Jing, H.W., Chen, S.J., Du, M.R., Chen, W.Q., & Duan, W.H. (2019). Influence of ultrasonication on the dispersion and enhancing effect of graphene oxide-carbon nanotube hybrid nanoreinforcement in cementitious composite. *Composites. Part B, Engineering*, 164, 45-53.
- Gong, K., Pan, Z., Korayem, A.H., Qiu, L., Li, D., Collins, F., Wang, C.M., & Duan, W.H. (2015). Reinforcing effects of graphene oxide on Portland cement paste. *Journal of Materials in Civil Engineering*, 27(2), A4014010. [http://dx.doi.org/10.1061/\(ASCE\)MT.1943-5533.0001125](http://dx.doi.org/10.1061/(ASCE)MT.1943-5533.0001125).
- Gordon, J.N., Pinnock, W.R., & Moore, M.M. (1996). A preliminary investigation of strength development in Jamaican red mud composites. *Cement and Concrete Composites*, 18(6), 371-379.
- Indukuri, C.S.R., Nerella, R., & Madduru, S.R.C. (2020). Workability, microstructure, strength properties and durability properties of graphene oxide reinforced cement paste. *Australian Journal of Civil Engineering*, 18(1), 73-81.
- IRC SP 20. (2002). Indian Road Congress for Rural Roads. In *Indian Road Congress* (pp. 1-2), India.
- IRC SP 89. (2010). IRC SP 89 part 1: guidelines for soil and granular material stabilization using cement, lime and fly ash. In *Indian Road Congress* (Vol. 53, No. 9, pp. 1689-1699), India.
- IRC SP 89. (2018). Guidelines for the design of stabilized pavements (part 2). In *Indian Road Congress*. India.
- Jha, A. K., Kumar, D., & Sivapullaiah, P. V. (2020). Influence of fly ash on geotechnical behavior of red mud: a micro-mechanistic study. *Geotechnical and Geological Engineering*, 38, 6157-6176.
- Kai, M.F., Zhang, L.W., & Liew, K.M. (2019). Graphene and graphene oxide in calcium silicate hydrates: chemical reactions, mechanical behavior, and interfacial sliding. *Carbon*, 146, 181-193.
- Kehagia, F. (2008). An innovative geotechnical application of bauxite residue. *Electronic Journal of Geotechnical Engineering*, 13, 1-9.
- Kumar, A., & Kumar, S. (2013). Development of paving blocks from synergistic use of red mud and fly ash using geopolymerization. *Construction & Building Materials*, 38, 865-871.
- Kumar, S., & Prasad, A. (2019). Parameters controlling strength of red mud-lime mix. *European Journal of Environmental and Civil Engineering*, 23(6), 743-757.
- Li, S., Zhang, J., Li, Z., Gao, Y., & Liu, C. (2021). Feasibility study of red mud-blast furnace slag based geopolymeric grouting material: effect of superplasticizers. *Construction & Building Materials*, 267, 120910.
- Lima, M.S.S., Thives, L.P., Haritonovs, V., & Bajars, K. (2017). Red mud application in construction industry: review of benefits and possibilities. *IOP Conference Series: Materials Science and Engineering*, 251(1), 012-033.
- Liu, J., Li, Q., & Xu, S. (2019). Reinforcing mechanism of graphene and graphene oxide sheets on cement-based materials. *Journal of Materials in Civil Engineering*, 31(4), 04019014.
- Liu, K., Zhang, K., Wu, J., Muhunthan, B., & Shi, X. (2018). Evaluation of mechanical performance and modification mechanism of asphalt modified with graphene oxide and warm mix additives. *Journal of Cleaner Production*, 193, 87-96.
- Mishra, M.C., Babu, K.S., Reddy, N.G., Dey, P.P., & Rao, B.H. (2019). Performance of lime stabilization on extremely alkaline red mud waste under acidic environment. *Journal of Hazardous, Toxic and Radioactive Waste*, 23(4), 04019012.
- Mishra, M.C., Gangadhara Reddy, N., Hanumantha Rao, B., & Kumar Das, S. (2020a). A Study on evaluating the usefulness and applicability of additives for neutralizing extremely alkaline red mud waste. In K.R. Reddy, A.K. Agnihotri, Y. Yukselen-Aksoy, B.K. Dubey & A. Bansal (Eds.), *Sustainable environmental geotechnics* (Lecture Notes in Civil Engineering, No. 89, pp. 139-149). Cham: Springer.
- Mishra, M.C., Reddy, N.G., & Rao, B.H. (2020b). Potential of citric acid for treatment of extremely alkaline bauxite residue: effect on geotechnical and geoenvironmental properties. *Journal of Hazardous, Toxic and Radioactive Waste*, 24(4), 04020047.
- Mohammed, A., Sanjayan, J.G., Duan, W.H., & Nazari, A. (2015). Incorporating graphene oxide in cement composites: a study of transport properties. *Construction & Building Materials*, 84, 341-347.
- Mohammed, A., Sanjayan, J.G., Duan, W.H., & Nazari, A. (2016). Graphene oxide impact on hardened cement expressed in enhanced freeze-thaw resistance. *Journal of Materials in Civil Engineering*, 28(9), 04016072.
- Naseri, F., Irani, M., & Dehkhodarajabi, M. (2016). Science Direct Effect of graphene oxide nanosheets on the

- geotechnical properties of cemented silty soil. *Archives of Civil and Mechanical Engineering. Politechnika Wroclawska*, 16(4), 695-701.
- Pateriya, A.S., Dharavath, K., & Robert, D.J. (2021). Enhancing the strength characteristics of No-fine concrete using wastes and nano materials. *Construction & Building Materials*, 276, 122222.
- Pateriya, A., Kishan, D., & Kushwaha, S.S. (2019). Evolution of the geotechnical properties of fly ash stabilized silty soil activated by Graphene Oxide (GO). *International Journal of Recent Technology and Engineering*, 8(2), 4732-4737.
- Priya, S.T., Mehra, A., Jain, S., & Kakria, K. (2021). Effect of graphene oxide on high-strength concrete induced with rice husk ash: mechanical and durability performance. *Innovative Infrastructure Solutions*, 6(1), 1-16.
- Reddy, M.S., Dinakar, P., & Rao, B.H. (2016a). A review of the influence of source material's oxide composition on the compressive strength of geopolymer concrete. *Microporous and Mesoporous Materials*, 234, 12-23.
- Reddy, N.G., & Rao, B.H. (2018). Compaction and consolidation behaviour of untreated and treated waste of Indian red mud. *Geotechnical Research*, 5(2), 106-121.
- Reddy, N.G., Chandra, S., & Rao, B.H. (2016b). Assessment of industrial wastes as a road construction material: a review assessment of industrial wastes as a road construction material: a review. In *Proceedings of 1st International Conference on Recent Innovations in Engineering and Technology (ICREIAT-2016)* (pp. 22-23), Bhalki.
- Reddy, N.G., Rao, B.H., & Reddy, K.R. (2018). Biopolymer amendment for mitigating dispersive characteristics of red mud waste. *Géotechnique Letters*, 8(3), 201-207. <http://dx.doi.org/10.1680/jgele.18.00033>.
- Reddy, N.G., Rao, B.H., & Reddy, K.R. (2019). Chemical analysis procedures for determining the dispersion behaviour of red mud. *Lecture Notes in Civil Engineering*, 32, 19-26.
- Reddy NG, Nongmaithem RS, Basu D, Rao BH. Application of biopolymers for improving the strength characteristics of red mud waste. *Environmental Geotechnics*. 2021a;9(6):340-59.
- Reddy, P.S., Reddy, N.G., Serjun, V.Z., Mohanty, B., Das, S.K., Reddy, K.R., & Rao, B.H. (2021b). Properties and assessment of applications of red mud (bauxite residue): current status and research needs. *Waste and Biomass Valorization*, 12(3), 1185-1217.
- Satayanarayana, P. V. V., Naidu, P. G., Adishesu, S., & Rao, CH. V. (2012). Characterization of lime stabilized red mud mix for feasibility in road construction. *International Journal of Engineering Research and Development*, 3(7), 20-26.
- Singh, S., Aswath, M.U., & Ranganath, R.V. (2020). Performance assessment of bricks and prisms: red mud-based geopolymer composite. *Journal of Building Engineering*, 32, 101462.
- Wan, H., & Zhang, Y. (2020). Interfacial bonding between graphene oxide and calcium silicate hydrate gel of ultra-high-performance concrete. *Materials and Structures*, 53(2), 34.
- Zhang, J., Liu, S., Yao, Z., Wu, S., Jiang, H., Liang, M., & Qiao, Y. (2018). Environmental aspects and pavement properties of red mud waste as the replacement of mineral filler in asphalt mixture. *Construction & Building Materials*, 180, 605-613.
- Zhang, J., Li, P., Liang, M., Jiang, H., Yao, Z., Zhang, X., & Yu, S. (2020a). Utilization of red mud as an alternative mineral filler in asphalt mastics to replace natural limestone powder. *Construction & Building Materials*, 237, 117821.
- Zhang, J., Yao, Z., Wang, K., Wang, F., Jiang, H., Liang, M., Wei, J., & Airey, G. (2020b). Sustainable utilization of bauxite residue (Red Mud) as a road material in pavements: a critical review. *Construction & Building Materials*, 270, 121419.
- Zhang, M., Zhao, M., Zhang, G., Mann, D., Lumsden, K., & Tao, M. (2016). Durability of red mud-fly ash based geopolymer and leaching behavior of heavy metals in sulfuric acid solutions and deionized water. *Construction & Building Materials*, 124, 373-382.
- Zhang, Z., & Tao, M. (2008). Durability of cement stabilized low plasticity soils. *Journal of Geotechnical and Geoenvironmental Engineering*, 134(2), 203-213.
- Zhao, M., Zhang, G., Htet, K.W., Kwon, M., Liu, C., Xu, Y., & Tao, M. (2019). Freeze-thaw durability of red mud slurry-class F fly ash-based geopolymer: effect of curing conditions. *Construction & Building Materials*, 215, 381-390.
- Zhao, Y., Liang, N.X., Chen, H., & Li, Y. (2020). Preparation and properties of sintering red mud unburned road brick using orthogonal experiments. *Construction & Building Materials*, 238, 117739.
- Zhu, B.Y., Murali, S., Cai, W., Li, X., Suk, J.W., Potts, J.R., & Ruoff, R.S. (2010). Graphene and graphene oxide: synthesis, properties, and applications. *Advanced Materials*, 22(35), 3906-3924.